Chapter 2

Aerodynamic Background

Flight dynamics deals principally with the response of aerospace vehicles to perturbations in their flight environments and to control inputs. In order to understand this response, it is necessary to characterize the aerodynamic and propulsive forces and moments acting on the vehicle, and the dependence of these forces and moments on the flight variables, including airspeed and vehicle orientation. These notes provide a simplified summary of important results from aerodynamics that can be used to characterize these dependencies.

2.1 Introduction

Flight dynamics deals with the response of aerospace vehicles to perturbations in their flight environments and to control inputs. Since it is changes in orientation (or *attitude*) that are most important, these responses are dominated by the generated aerodynamic and propulsive moments. For most aerospace vehicles, these moments are due largely to changes in the lifting forces on the vehicle (as opposed to the drag forces that are important in determining performance). Thus, in some ways, the prediction of flight stability and control is easier than the prediction of performance, since these lifting forces can often be predicted to within sufficient accuracy using inviscid, linear theories.

In these notes, I attempt to provide a uniform background in the aerodynamic theories that can be used to analyze the stability and control of flight vehicles. This background is equivalent to that usually covered in an introductory aeronautics course, such as one that might use the text by Shevell [6]. This material is often reviewed in flight dynamics texts; the material presented here is derived, in part, from the material in Chapter 1 of the text by Seckel [5], supplemented with some of the material from Appendix B of the text by Etkin & Reid [3]. The theoretical basis for these linear theories can be found in the book by Ashley & Landahl [2].

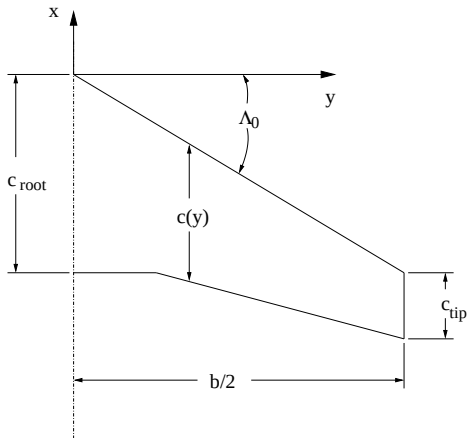

Figure 2.1: Planform geometry of a typical lifting surface (wing).

2.2 Lifting surface geometry and nomenclature

We begin by considering the geometrical parameters describing a lifting surface, such as a wing or horizontal tail plane. The projection of the wing geometry onto the x-y plane is called the wing *planform*. A typical wing planform is sketched in Fig. 2.1. As shown in the sketch, the maximum lateral extent of the planform is called the wing span b, and the area of the planform S is called the wing area.

The wing area can be computed if the spanwise distribution of local section chord $c(y)$ is known using

$$S = \int_{-b/2}^{b/2} c(y)\,\mathrm{d}y = 2\int_{0}^{b/2} c(y)\,\mathrm{d}y, \tag{2.1}$$

where the latter form assumes bi-lateral symmetry for the wing (the usual case). While the span characterizes the lateral extent of the aerodynamic forces acting on the wing, the *mean aerodynamic chord* $\bar{c}$ characterizes the axial extent of these forces. The mean aerodynamic chord is usually approximated (to good accuracy) by the *mean geometric chord*

$$\bar{c} = \frac{2}{S}\int_{0}^{b/2} c^2\,\mathrm{d}y \tag{2.2}$$

The dimensionless ratio of the span to the mean chord is also an important parameter, but instead of using the ratio $b/\bar{c}$ the *aspect ratio* of the planform is defined as

$$\mathbf{AR} \equiv \frac{b^2}{S} \tag{2.3}$$

Note that this definition reduces to the ratio b/c for the simple case of a wing of rectangular planform (having constant chord c).

The lift, drag, and pitching moment coefficients of the wing are defined as

$$\begin{aligned} \mathbf{C}_L &= \frac{L}{QS} \\ \mathbf{C}_D &= \frac{D}{QS} \\ \mathbf{C}_m &= \frac{M}{QS\bar{c}} \end{aligned} \tag{2.4}$$

where

$$Q = \frac{\rho V^2}{2}$$

is the dynamic pressure, and L, D, M are the lift force, drag force, and pitching moment, respectively, due to the aerodynamic forces acting on the wing.

Conceptually, and often analytically, it is useful to build up the aerodynamic properties of lifting surfaces as integrals of sectional properties. A wing section, or *airfoil*, is simply a cut through the lifting surface in a plane of constant y. The lift, drag, and pitching moment coefficients of the airfoil section are defined as

$$\begin{aligned} \mathbf{c}_\ell &= \frac{\ell}{Q\bar{c}} \\ \mathbf{C}_d &= \frac{d}{Q\bar{c}} \\ \mathbf{C}_{m\text{sect}} &= \frac{m}{Q\bar{c}^2} \end{aligned} \tag{2.5}$$

where ℓ, d, and m are the lift force, drag force, and pitching moment, per unit span, respectively, due to the aerodynamics forces acting on the airfoil section. Note that if we calculate the wing lift coefficient as the chord-weighted average integral of the section lift coefficients

$$\mathbf{C}_L = \frac{2}{S}\int_0^{b/s} \mathbf{c}_\ell c \,\mathrm{d}y \tag{2.6}$$

for a wing with *constant* section lift coefficient, then Eq. (2.6) gives

$$\mathbf{C}_L = \mathbf{c}_\ell$$

2.2.1 Geometric properties of trapezoidal wings

The planform shape of many wings can be approximated as trapezoidal. In this case, the root chord c_{root}, tip chord c_{tip}, span b, and the sweep angle of any constant-chord fraction Λ_n completely specify the planform. Usually, the geometry is specified in terms of the wing taper ratio $\lambda = c_{\text{tip}}/c_{\text{root}}$; then using the geometric properties of a trapezoid, we have

$$S = \frac{c_{\text{root}}(1+\lambda)}{2} b \tag{2.7}$$

and

$$\mathbf{AR} = \frac{2b}{c_{\text{root}}(1+\lambda)} \tag{2.8}$$

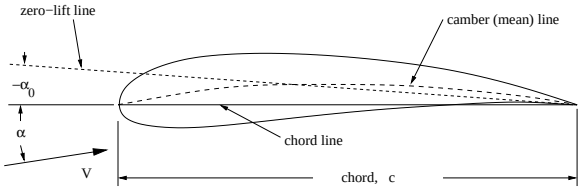

Figure 2.2: Geometry of a typical airfoil section.

The local chord is then given as a function of the span variable by

$$c = c_{\text{root}} \left[1 - (1-\lambda)\frac{2y}{b} \right] \tag{2.9}$$

and substitution of this into Eq. (2.2) and carrying out the integration gives

$$\bar{c} = \frac{2(1+\lambda+\lambda^2)}{3(1+\lambda)} c_{\text{root}} \tag{2.10}$$

The sweep angle of any constant-chord fraction line can be related to that of the leading-edge sweep angle by

$$\mathbf{AR} \tan\Lambda_n = \mathbf{AR} \tan\Lambda_0 - 4n\frac{1-\lambda}{1+\lambda} \tag{2.11}$$

where $0 \le n \le 1$ is the chord fraction (e.g., 0 for the leading edge, 1/4 for the quarter-chord line, etc.). Finally, the location of any chord-fraction point on the mean aerodynamic chord, relative to the wing apex, can be determined as

$$\begin{aligned} \bar{x}_n = \frac{2}{S}\int_0^{b/2} x_n c \, \mathrm{d}y &= \frac{2}{S}\int_0^{b/2} (nc_{\text{root}} + y\tan\Lambda_n) \, \mathrm{d}y \\ &= \frac{3(1+\lambda)\bar{c}}{2(1+\lambda+\lambda^2)} \left\{ n + \left(\frac{1+2\lambda}{12} \right) \mathbf{AR} \tan\Lambda_n \right\} \end{aligned} \tag{2.12}$$

Alternatively, we can use Eq. (2.11) to express this result in terms of the leading-edge sweep as

$$\frac{\bar{x}_n}{\bar{c}} = n + \frac{(1+\lambda)(1+2\lambda)}{8(1+\lambda+\lambda^2)} \mathbf{AR} \tan\Lambda_0 \tag{2.13}$$

Substitution of $n = 0$ (or $n = 1/4$) into either Eq. (2.12) or Eq. (2.13) gives the axial location of the leading edge (or quarter-chord point) of the mean aerodynamic chord relative to the wing apex.

2.3 Aerodynamic properties of airfoils

The basic features of a typical airfoil section are sketched in Fig. 2.2. The longest straight line from the trailing edge to a point on the leading edge of the contour defines the *chord line*. The length of this line is called simply the *chord c*. The locus of points midway between the upper and lower surfaces is called the mean line, or *camber line*. For a symmetric airfoil, the camber and chord lines coincide.

For low speeds (i.e., Mach numbers $\mathbf{M} << 1$), and at high Reynolds numbers $\mathbf{Re} = Vc/\nu >> 1$, the results of thin-airfoil theory predict the lifting properties of airfoils quite accurately for angles of attack not too near the stall. Thin-airfoil theory predicts a linear relationship between the section lift coefficient and the angle of attack α of the form

$$\mathbf{c}_\ell = a_0 \left(\alpha - \alpha_0\right) \tag{2.14}$$

as shown in Fig. 2.3. The theory also predicts the value of the lift-curve slope

$$a_0 = \frac{\partial \mathbf{c}_\ell}{\partial \alpha} = 2\pi \tag{2.15}$$

Thickness effects (not accounted for in thin-airfoil theory) tend to increase the value of a_0, while viscous effects (also neglected in the theory) tend to decrease the value of a_0. The value of a_0 for realistic conditions is, as a result of these counter-balancing effects, remarkably close to 2π for most practical airfoil shapes at the high Reynolds numbers of practical flight.

The angle α_0 is called the *angle for zero lift*, and is a function only of the shape of the camber line. Increasing (conventional, sub-sonic) camber makes the angle for zero lift α_0 increasingly negative. For camber lines of a given family (i.e., shape), the angle for zero lift is very nearly proportional to the magnitude of camber – i.e., to the maximum deviation of the camber line from the chord line.

A second important result from thin-airfoil theory concerns the location of the *aerodynamic center*. The aerodynamic center of an airfoil is the point about which the pitching moment, due to the distribution of aerodynamic forces acting on the airfoil surface, is independent of the angle of attack. Thin-airfoil theory tells us that the aerodynamic center is located on the chord line, one quarter of the way from the leading to the trailing edge – the so-called *quarter-chord* point. The value of the pitching moment about the aerodynamic center can also be determined from thin-airfoil theory, but requires a detailed calculation for each specific shape of camber line. Here, we simply note that, for a given shape of camber line the pitching moment about the aerodynamic center is proportional to the amplitude of the camber, and generally is negative for conventional subsonic (concave down) camber shapes.

It is worth emphasizing that thin-airfoil theory neglects the effects of viscosity and, therefore, cannot predict the behavior of airfoil stall, which is due to boundary layer separation at high angles of attack. Nevertheless, for the angles of attack usually encountered in controlled flight, it provides a very useful approximation for the lift.

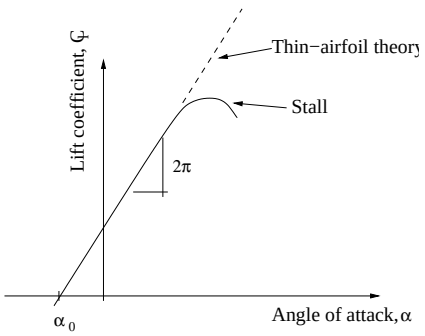

Figure 2.3: Airfoil section lift coefficient as a function of angle of attack.

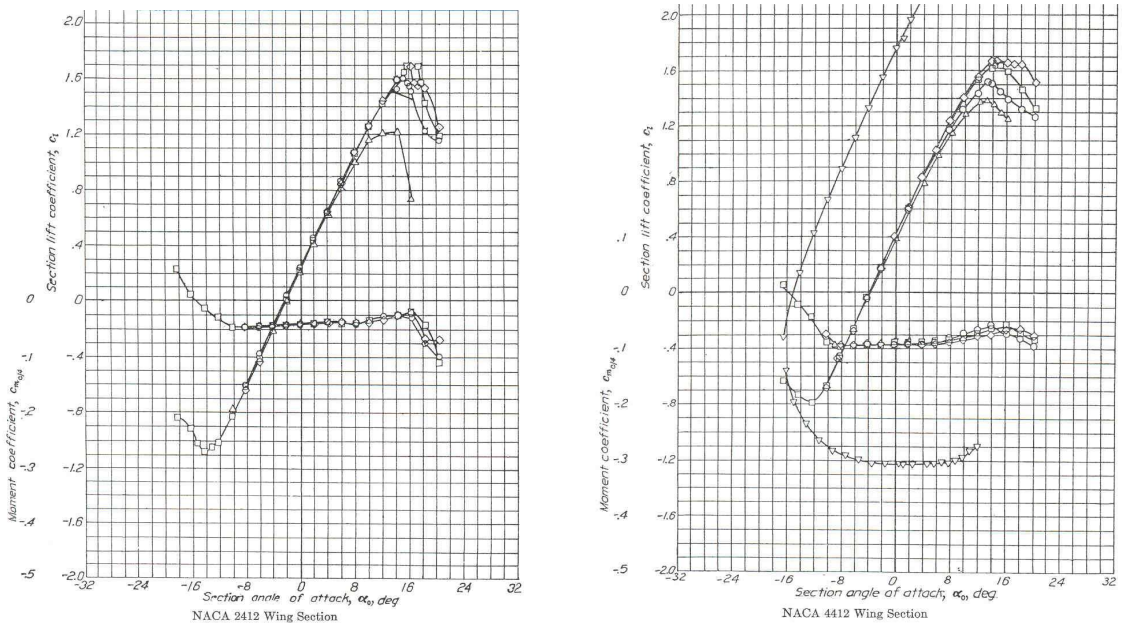

Figure 2.4: Airfoil lift and moment coefficients as a function of angle of attack; wind tunnel data for two cambered airfoil sections. Data from Abbott & von Doenhoff [1].

Finally, wind tunnel data for two cambered airfoil sections are presented in Fig. 2.4. Both airfoils have the same thickness distributions and camber line shapes, but the airfoil on the right has twice as much camber as the one on the left (corresponding to 4 per cent chord, versus 2 per cent for the airfoil on the left). The several curves correspond to Reynolds numbers ranging from $\mathbf{Re} = 3 \times 10^6$ to $\mathbf{Re} = 9 \times 10^6$, with the curves having larger values of $\mathbf{c}_{\ell_{\max}}$ corresponding to the higher Reynolds numbers. The outlying curves in the plot on the right correspond to data taken with a 20 per cent chord split flap deflected (and are not of interest here).

Note that these data are generally consistent with the results of thin-airfoil theory. In particular:

1. The lift-curve slopes are within about 95 per cent of the value of $a_0 = 2\pi$ over a significant range of angles of attack. Note that the angles of attack in Fig. 2.4 are in degrees, whereas the $a_0 = 2\pi$ is *per radian*;

2. The angle for zero lift of the section having the larger camber is approximately twice that of the section having the smaller camber; and

3. The moment coefficients measured about the quarter-chord point are very nearly independent of angle of attack, and are roughly twice as large for the airfoil having the larger camber.

2.4 Aerodynamic properties of finite wings

The vortex structures trailing downstream of a finite wing produce an induced downwash field near the wing which can be characterized by an *induced angle of attack*

$$\alpha_i = \frac{\mathbf{C}_L}{\pi e \mathbf{AR}} \tag{2.16}$$

For a straight (un-swept) wing with an elliptical spanwise loading, lifting-line theory predicts that the induced angle of attack α_i is constant across the span of the wing, and the *efficiency factor* $e = 1.0$. For non-elliptical span loadings, $e < 1.0$, but for most practical wings α_i is still nearly constant across the span. Thus, for a finite wing lifting-line theory predicts that

$$\mathbf{C}_L = a_0 \left(\alpha - \alpha_0 - \alpha_i\right) \tag{2.17}$$

where a_0 is the wing section lift-curve slope and α_0 is the angle for zero lift of the section. Substituting Eq. (2.16) and solving for the lift coefficient gives

$$\mathbf{C}_L = \frac{a_0}{1 + \frac{a_0}{\pi e \mathbf{AR}}}(\alpha - \alpha_0) = a(\alpha - \alpha_0) \tag{2.18}$$

whence the *wing* lift-curve slope is given by

$$a = \frac{\partial \mathbf{C}_L}{\partial \alpha} = \frac{a_0}{1 + \frac{a_0}{\pi e \mathbf{AR}}} \tag{2.19}$$

Lifting-line theory is asymptotically correct in the limit of large aspect ratio, so, in principle, Eq. (2.18) is valid only in the limit as $\mathbf{AR} \to \infty$. At the same time, slender-body theory is valid in the limit of vanishingly small aspect ratio, and it predicts, independently of planform shape, that the lift-curve slope is

$$a = \frac{\pi \mathbf{AR}}{2} \tag{2.20}$$

Note that this is one-half the value predicted by the limit of the lifting-line result, Eq. (2.19), as the aspect ratio goes to zero. We can construct a single empirical formula that contains the correct limits for both large and small aspect ratio of the form

$$a = \frac{\pi \mathbf{AR}}{1 + \sqrt{1 + \left(\frac{\pi \mathbf{AR}}{a_0}\right)^2}} \tag{2.21}$$

A plot of this equation, and of the lifting-line and slender-body theory results, is shown in Fig. 2.5.

Equation (2.21) can also be modified to account for wing sweep and the effects of compressibility. If the sweep of the quarter-chord line of the planform is $\Lambda_{c/4}$, the effective section incidence is increased by the factor $1/\cos\Lambda_{c/4}$, relative to that of the wing,[1] while the dynamic pressure of the flow normal to the quarter-chord line is reduced by the factor $\cos^2\Lambda_{c/4}$. The section lift-curve slope is thus reduced by the factor $\cos\Lambda_{c/4}$, and a version of Eq. (2.21) that accounts for sweep can be written

$$a = \frac{\pi \mathbf{AR}}{1 + \sqrt{1 + \left(\frac{\pi \mathbf{AR}}{a_0 \cos\Lambda_{c/4}}\right)^2}} \tag{2.22}$$

[1] This factor can best be understood by interpreting a change in angle of attack as a change in vertical velocity $\Delta w = V_\infty \, \Delta\alpha$.

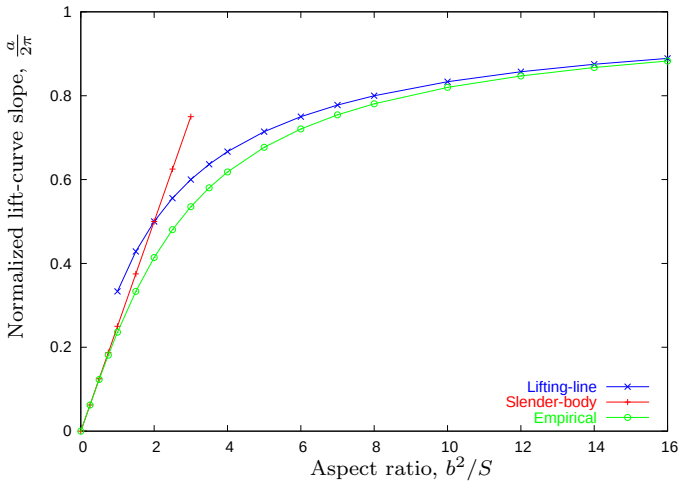

Figure 2.5: Empirical formula for lift-curve slope of a finite wing compared with lifting-line and slender-body limits. Plot is constructed assuming $a_0 = 2\pi$.

Finally, for subcritical ($\mathbf{M}_\infty < \mathbf{M}_{\text{crit}}$) flows, the Prandtl-Glauert similarity law for airfoil sections gives

$$a_{2\text{d}} = \frac{a_0}{\sqrt{1 - \mathbf{M}_\infty^2}} \tag{2.23}$$

where $\mathbf{M}_\infty$ is the flight Mach number. The Goethert similarity rule for three-dimensional wings modifies Eq. (2.22) to the form

$$a = \frac{\pi \mathbf{AR}}{1 + \sqrt{1 + \left(\frac{\pi \mathbf{AR}}{a_0 \cos \Lambda_{c/4}}\right)^2 \left(1 - \mathbf{M}_\infty^2 \cos^2 \Lambda_{c/4}\right)}} \tag{2.24}$$

In Eqs. (2.22), (2.23) and (2.24), a_0 is, as earlier, the incompressible, two-dimensional value of the lift-curve slope (often approximated as $a_0 = 2\pi$). Note that, according to Eq. (2.24) the lift-curve slope increases with increasing Mach number, but not as fast as the two-dimensional Prandtl-Glauert rule suggests. Also, unlike the Prandtl-Glauert result, the transonic limit ($\mathbf{M}_\infty \cos \Lambda_{c/4} \to 1.0$) is finite and corresponds (correctly) to the slender-body limit.

So far we have described only the lift-curve slope $a = \partial \mathbf{C}_L / \partial \alpha$ for the finite wing, which is its most important parameter as far as stability is concerned. To determine trim, however, it is also important to know the value of the pitching moment at zero lift (which is, of course, also equal to the pitching moment about the aerodynamic center). We first determine the angle of attack for wing zero lift. From the sketch in Fig. 2.6, we see that the angle of attack measured at the wing root corresponding to zero lift at a given section can be written

$$-(\alpha_0)_{\text{root}} = \epsilon - \alpha_0 \tag{2.25}$$

where ϵ is the geometric twist at the section, relative to the root. The wing lift coefficient can then be expressed as

$$\mathbf{C}_L = \frac{2}{S} \int_0^{b/2} a \left[\alpha_r - (\alpha_0)_{\text{root}}\right] c \, \mathrm{d}y = \frac{2a}{S} \left[\frac{S}{2} \alpha_r + \int_0^{b/2} (\epsilon - \alpha_0) \, c \, \mathrm{d}y\right] \tag{2.26}$$

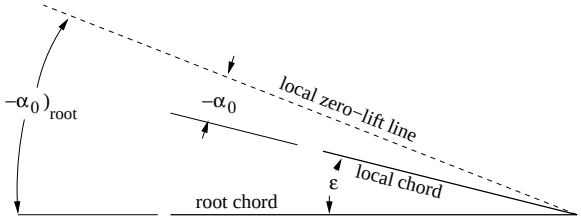

Figure 2.6: Root angle of attack corresponding to zero lift at a given section.

Setting the lift coefficient to zero and solving for the root angle of attack then yields

$$(\alpha_r)_{L=0} = \frac{2}{S}\int_0^{b/2} (\alpha_0 - \epsilon)\, c\, \mathrm{d}y \tag{2.27}$$

Now, the wing pitching moment about its aerodynamic center can be determined as the sum of contributions from the section values plus the contribution due to the *basic* lift distribution – i.e., the distribution of lifting forces at wing zero lift.[2]These contributions can be expressed as

$$\mathbf{C}_{mac} = \frac{2}{S\bar{c}}\left\{\int_0^{b/2} c^2 \left(\mathbf{C}_{mac}\right)_{\text{sect}}\, \mathrm{d}y + \int_0^{b/2} a\left[(\alpha_r)_{L=0} + \epsilon - \alpha_0\right] c x_1\, \mathrm{d}y\right\} \tag{2.28}$$

where $x_1 = x_{ac} - x_{MAC}$ is the axial distance between the section aerodynamic center and the wing aerodynamic center. Consistent with these approximations, the wing aerodynamic center is located at the chord-weighted quarter-chord location for the wing; i.e.,

$$x_{MAC} = \frac{2}{S}\int_0^{b/2} x_{c/4} c\, \mathrm{d}y \tag{2.29}$$

Explicit expressions for this variable can be determined from Eqs. (2.12,2.13) for wings of trapezoidal planform.

2.5 Fuselage contribution to pitch stiffness

The contribution of the fuselage to the pitching moment is affected by interference effects with the wing flow field. These can be estimated using a simple strip theory (as described, for example, in Example 2.2 of the text by Nelson [4]), but here we will introduce a simple estimate for the destabilizing effect of the fuselage in the absence of interference effects.

Slender-body theory predicts a distribution of lifting force given by

$$\frac{\mathrm{d}L}{\mathrm{d}x} = 2Q\alpha\frac{\mathrm{d}S_f}{\mathrm{d}x} \tag{2.30}$$

where $S_f = \pi w^2/4$ is the equivalent cross-sectional area of the fuselage based on its width w as a function of the streamwise variable x. For a finite-length fuselage, Eq. (2.30) predicts positive lift on

[2]The basic lift distribution, of course, sums to zero lift, but is still capable of producing non-zero pitching moments when the wing is swept.

the forward part of the fuselage (where S_f is generally increasing), and negative lift on the rearward part (where S_f is generally decreasing), but the total lift is identically zero (since $S_f(0) = S_f(\ell_f) = 0$, where ℓ_f is the fuselage length).

Since the total lift acting on the fuselage is zero, the resulting force system is a pure couple, and the pitching moment will be the same, regardless of the reference point about which it is taken. Thus, e.g., taking the moment about the fuselage nose ($x = 0$), we have

$$M_f = -\int_0^{\ell_f} x \, \mathrm{d}L = -2Q\alpha \int_0^{\ell_f} x \, \mathrm{d}S_f = 2Q\alpha \int_0^{\ell_f} S_f \, \mathrm{d}x = 2Q\alpha\mathcal{V} \tag{2.31}$$

where $\mathcal{V}$ is the volume of the "equivalent" fuselage (i.e., the body having the same planform as the actual fuselage, but with circular cross-sections). The fuselage contribution to the vehicle pitching moment coefficient is then

$$\mathbf{C}_m = \frac{M_f}{QS\bar{c}} = \frac{2\mathcal{V}}{S\bar{c}}\alpha \tag{2.32}$$

and the corresponding pitch stiffness is

$$\mathbf{C}_{m\alpha} = \left(\frac{\partial \mathbf{C}_m}{\partial \alpha}\right)_{\text{fuse}} = \frac{2\mathcal{V}}{S\bar{c}} \tag{2.33}$$

Note that this is always positive – i.e., destabilizing.

2.6 Wing-tail interference

The one interference effect we will account for is that between the wing and the horizontal tail. Because the tail operates in the downwash field of the wing (for conventional, aft-tail configurations), the effective angle of attack of the tail is reduced. The reduction in angle of attack can be estimated to be

$$\varepsilon = \kappa \frac{\mathbf{C}_L}{\pi e \mathbf{AR}} \tag{2.34}$$

where $1 < \kappa < 2$. Note that $\kappa = 1$ corresponds to $\varepsilon = \alpha_i$, the induced angle of attack of the wing, while $\kappa = 2$ corresponds to the limit when the tail is far downstream of the wing. For stability considerations, it is the rate of change of tail downwash with angle of attack that is most important, and this can be estimated as

$$\frac{\mathrm{d}\varepsilon}{\mathrm{d}\alpha} = \frac{\kappa}{\pi e \mathbf{AR}} \left(\mathbf{C}_{L\alpha}\right)_{\text{wing}} \tag{2.35}$$

2.7 Control Surfaces

Aerodynamic control surfaces are usually trailing-edge flaps on lifting surfaces that can be deflected by control input from the pilot (or autopilot). Changes in camber line slope near the trailing edge of a lifting surface are very effective at generating lift. The lifting pressure difference due to trailing-edge flap deflection on a two-dimensional airfoil, calculated according to thin-airfoil theory, is plotted in Fig. 2.7 (a) for flap chord lengths of 10, 20, and 30 percent of the airfoil chord. The values plotted

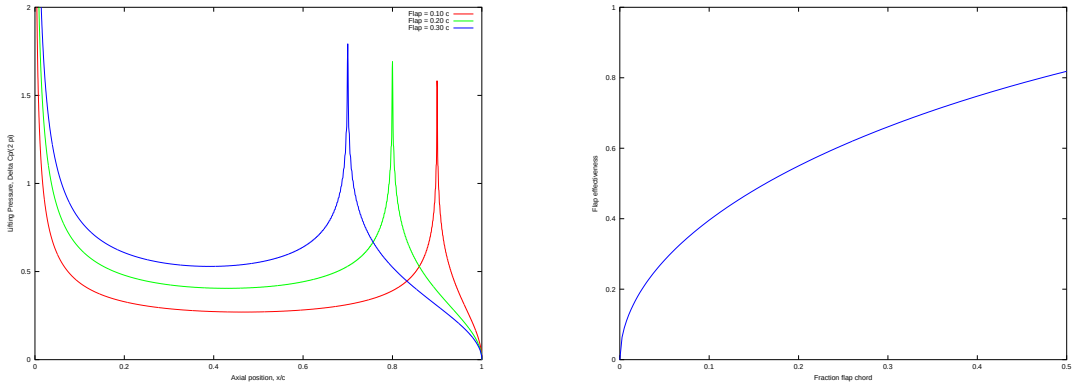

(a) Lifting pressure coefficient (b) Control effectiveness

Figure 2.7: Lifting pressure distribution due to flap deflection and resulting control effectiveness.

are per unit angular deflection, and normalized by 2π, so their integrals can be compared with the changes due to increments in angle of attack. Figure 2.7 (b) shows the *control effectiveness*

$$\frac{\partial \mathbf{C}_\ell}{\partial \delta} \tag{2.36}$$

also normalized by 2π. It is seen from this latter figure that deflection of a flap that consists of only 25 percent chord is capable of generating about 60 percent of the lift of the entire airfoil pitched through an angle of attack equal to that of the flap deflection. Actual flap effectiveness is, of course, reduced somewhat from these ideal values by the presence of viscous effects near the airfoil trailing edge, but the flap effectiveness is still nearly 50 percent of the lift-curve slope for a 25 percent chord flap for most actual flap designs.

The control forces required to change the flap angle are related to the aerodynamic moments about the hinge-line of the flap. The aerodynamic moment about the hinge line is usually expressed in terms of the dimensionless hinge moment coefficient, e.g., for the elevator hinge moment H_e, defined as

$$\mathbf{C}_{h_e} \equiv \frac{H_e}{\frac{1}{2}\rho V^2 S_e c_e} \tag{2.37}$$

where S_e and c_e are the elevator planform area and chord length, respectively; these are based on the area of the control surface aft of the hinge line.

The most important characteristics related to the hinge moments are the restoring tendency and the floating tendency. The *restoring tendency* is the derivative of the hinge moment coefficient with respect to control deflection; e.g., for the elevator,

$$\mathbf{C}_{h_{\delta_e}} = \frac{\partial \mathbf{C}_{h_e}}{\partial \delta_e} \tag{2.38}$$

The *floating tendency* is the derivative of the hinge moment coefficient with respect to angle of attack; e.g., for the elevator,

$$\mathbf{C}_{h_{e_{\alpha_t}}} = \frac{\partial \mathbf{C}_{h_e}}{\partial \alpha_t} \tag{2.39}$$

where α_t is the angle of attack of the tail.

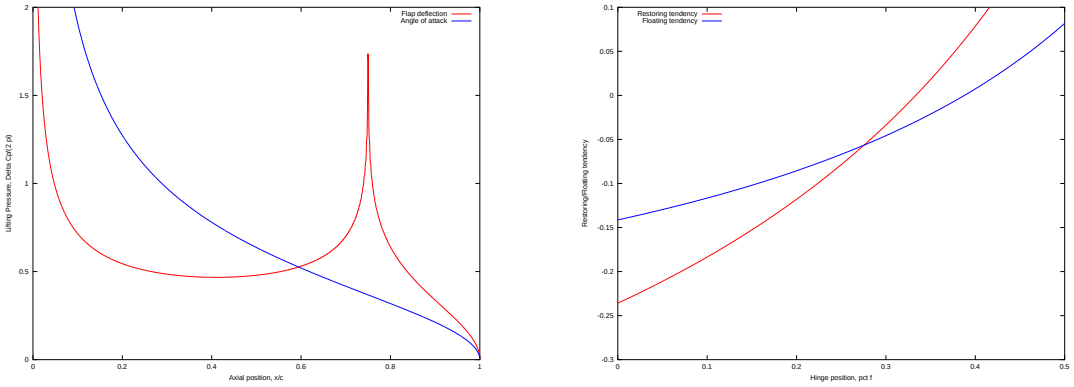

(a) Lifting pressure coefficient

(b) Hinge moment derivatives

Figure 2.8: Lifting pressure distributions (normalized by 2π) due to flap deflection and to change in angle of attack, and resulting restoring and floating tendencies of control flap. Results of thin-airfoil theory for 25 percent chord trailing-edge flap.

The restoring and floating tendencies are due primarily to the moments produced about the control flap hinge line by the lifting pressures induced by changes in either control position or angle of attack. The thin-airfoil approximations to these lifting pressure distributions are illustrated in Fig. 2.8 (a) for a 25 percent chord trailing edge flap. The plotted values of $\mathbf{\Delta C}_p$ are normalized by 2π, so the average value of the $\mathbf{\Delta C}_p$ due to angle of attack change is unity (corresponding to a lift curve slope of 2π). Figure 2.8 (b) illustrates the corresponding floating and restoring tendencies as functions of the hinge line location, measured in fraction of flap chord. It is seen that both tendencies are negative for hinge lines located ahead of approximately the 33 percent flap chord station. While these results, based on inviscid, thin-airfoil theory are qualitatively correct, actual hinge moment coefficients are affected by viscous effects and leakage of flow between the flap and the main lifting surface, so the results presented here should be used only as a guide to intuition.

Bibliography

[1] Ira H. Abbott & Albert E. von Doenhoff, **Theory of Wing Sections; Including a Summary of Data**, Dover, New York, 1958.

[2] Holt Ashley & Marten Landahl, **Aerodynamics of Wings and Bodies**, Addison-Wesley, Reading, Massachusetts, 1965.

[3] Bernard Etkin & Lloyd D. Reid, **Dynamics of Flight; Stability and Control**, John Wiley & Sons, New York, Third Edition, 1998.

[4] Robert C. Nelson, **Flight Stability and Automatic Control**, McGraw-Hill, New York, Second Edition, 1998.

[5] Edward Seckel, **Stability and Control of Airplanes and Helicopters**, Academic Press, New York, 1964.

[6] Richard Shevell, **Fundamentals of Flight**, Prentice Hall, Englewood Cliffs, New Jersey, Second Edition, 1989.